Available online at www.sciencedirect.com
SCIENCE DIRECT
Journal of Chromatography A, 1104 (2006) 272–281
JOURNAL OF CHROMATOGRAPHY A
www.elsevier.com/locate/chroma

Size fractionation and characterization of natural colloids by flow-field flow fractionation coupled to multi-angle laser light scattering

M. Baalousha [a,*], F.V.D. Kammer [b], M. Motelica-Heino [c], H.S. Hilal [d], P. Le Coustumer [a,**]

[a] *University of Bordeaux 1, Center of Development of Applied Geology, Avenue des Facultés, 33400 Talence, France*
[b] *Technical University of Hamburg-Harburg, Department of Environmental Science and Technology, Eissendorfer Strasse 40, 21073 Hamburg, Germany*
[c] *BRGM, Avenue Claude Guillemin, 45060 Orléans, France*
[d] *Department of Chemistry, An-Najah N. University, PO Box 7, Nablus, Palestine*

Received 11 October 2004; received in revised form 23 November 2005; accepted 28 November 2005
Available online 19 December 2005

Abstract

Flow-field flow fractionation (FlFFF) coupled to multi-angle laser light scattering (MALLS) was evaluated for size and shape determination of standard spherical and arbitrarily shaped natural colloids. Different fitting methods for light scattering data retrieved from MALLS were evaluated to determine the particle size of spherical standards and natural colloids. In addition, FlFFF was optimized for best fractionation in connection to MALLS, minimal colloids-membrane interaction, and minimal sample losses. FlFFF, calibrated with standard particles, was used to determine hydrodynamic diameter, or radius (D_h or R_h), of the fractionated colloids, whereas the MALLS was used to determine root mean square radius of gyration (R_g) for fractionated colloids. Combining both results, by calculating the R_g/R_h ratio, allows an estimation of colloid deviation from the shape of homogeneous sphere. Accordingly, this study demonstrates that, FlFFF–MALLS is a valuable technique for characterizing heterogeneous and arbitrarily shaped natural colloidal particles in terms of size and shape. To check the usefulness of FlFFF–MALLS in natural colloid studies, the technique was used to investigate the sedimentation behavior of extracted soil colloidal particles. Results illustrate that, in a silty till sample, carbonates function as cement between the colloidal particles, and consequently, change their sedimentation behavior. On the other hand, carbonate dissolution generates a more homogeneous colloidal sample.

Keywords: FlFFF; MALLS; Natural colloids; RMS radius of gyration; Hydrodynamic radius; Particle shape

1. Introduction

Colloids play an important role in the aquatic environment such as contaminant adsorption, transport and sedimentation [1–6]. Colloid size and shape are the dominant parameters that control their mobility and interaction with other environmental chemical species [7–8]. This is because such interactions depend on the colloidal surface area, and consequently, on their size and shape.

To better understand the role of colloids in the environment, it is necessary to thoroughly characterize their size, size distribution, and shape. Natural colloidal systems normally show broad size distributions (1–1000 nm) and diverse shapes (spherical, platelet, rod, etc.). Understanding the role of colloids in the environment is limited by the lack of efficient methods to fractionate and characterize them [9]. FIFFF is a prominent technique for colloid fractionation [10–18]. For further analysis of the fractionated colloids, FIFFF has been coupled to several detectors such as UV–vis, MALLS [11], graphite furnace atomic absorption spectroscopy (GFAAS) [12], inductively coupled plasma-mass spectroscopy (ICP-MS) [12–16], electrothermal atomic absorption spectroscopy (ETAAS) [17] or scanning electron microscopy (SEM) [18]. These techniques allow determining: colloid size distribution, shape, chemical composition, and interaction with contaminants [19].

FlFFF is a separation technique based on hydrodynamic principles in which particles are separated due to their interaction with the cross-flow-field force (friction coefficient) and their translational diffusion. Within a thin channel, a parabolic flow profile is generated by the carrier flow. The cross-flow operates perpendicular to the carrier flow and drives the particles to the

* Corresponding author. Tel.: +33 540008798; fax: +33 556807138.
** Corresponding author.
E-mail addresses: mbalousha@yahoo.co.uk, m.baalousha@cdga.u-bordeaux1.fr (M. Baalousha).

0021-9673/$ – see front matter © 2005 Published by Elsevier B.V.
doi:10.1016/j.chroma.2005.11.095

bottom of the channel (the accumulation wall, which is in general an ultrafiltration membrane). The translational diffusion of the particles causes them to migrate back into the channel against the applied cross-flow. At equilibrium, the two motions are balanced. The smaller, highly diffusive, particles form clouds which stretch, further into the channel than the larger low-diffusive particles do. Due to the parabolic flow profile of the carrier flow, smaller particles experience higher flow rates (on the average) than larger ones. In this normal fractionation mode, the particle retention is a function of its apparent diffusion coefficient. Hence, the particle retention volume can be related to its diffusion coefficient, and consequently, to its hydrodynamic diameter (D_h) or radius (R_h) using the Stoke's equation. The conversion of the retention volume to hydrodynamic radius can be accomplished either by calculating channel parameters and applying FlFFF theory [20–22], or by calibrating with standard spherical particles of known size. In analyzing a non-spherical particle, the observed R_h is approximated as a radius of a sphere having similar hydrodynamic behavior in terms of diffusion and friction. FlFFF theory rigors are described elsewhere [10,18–22] and need not be concerned here.

It is common to use UV–vis detector signals, following FlFFF, to study particle mass distributions [10,12,19]. However, in solid particles, light attenuation is affected by light scattering. Therefore, light attenuation is influenced by parameters other than particle mass concentration such as: size, shape, composition, and refractive index. UV–vis is non-quantitative when applied to polydispersed spherical particles (latex beads) without correction for light scattering effects [23]. However, when UV–vis is applied to heterogeneous natural particles, there are strong indications that the UV–vis is a good approximation of particles mass concentration [12]. In this study, a fluorescence detector (FLD) was used as a 90° light scattering detector by setting the excitation wavelength equal to the emission wavelength. This principle, the so-called *nephelometric* turbidity detection, is stipulated by US-EPA for the determination of turbidity in water samples since it is much less affected by the true light absorbing substances [24]. Signals obtained by FLD are comparable to those obtained by UV–vis without any interference by light absorption from organic material, e.g. humic substances. The same considerations for UV–vis detection should be applied. Further, multi-angle laser light scattering (MALLS) was used to determine colloidal size. It allows the determination of particle root mean square radius of gyration (R_g) by measuring the net intensity of light scattered by such particles at a range of fixed angles. The particle R_g is determined by the mass distribution within the particle. The single mass increments are weighted by the square of the radius distance from the center of mass. Consequently, two particles with same hydrodynamic radius (R_h), but with different R_g values, may have a different mass distribution, and thus, different shapes. Combining the two sizing techniques via R_g/R_h ratios, particle shapes may be determined.

Interferences inside the FlFFF channel during the fractionation process such as: overload effects, steric elution mode, particle–wall interactions, and shape selective retention, are frequently observed with natural samples, resulting in non-ideal elution behavior. More accurate results may be obtained by measuring the colloidal size independently of the FlFFF fractionation. FlFFF–MALLS is a method of choice for the accurate determination of colloidal size and size distribution as it overcomes the problems arising in either of them separately. FlFFF allows colloids size fractionation and R_h determination. Moreover, it provides colloid pre-fractionation. Therefore, MALLS is performed on fractions with lower heterogeneity/polydispersity than the bulk sample. Thus, MALLS provides an evaluation of the FlFFF fractionation. It allows the determination of particle root mean square radius of gyration (R_g) by measuring the net intensity of light scattered by such particles at a range of fixed angles. The particle R_g is determined by the mass distribution within the particle. The single mass increments are weighted by the square of the radius distance from the center of mass. Consequently, two particles with same hydrodynamic radius (R_h), but with different R_g values, may have a different mass distribution, and most likely, different shapes. Combining the two sizing techniques via R_g/R_h ratios, particle shapes may be determined [27].

The main goal of this work is to demonstrate the applicability and benefits of FlFFF–MALLS in natural colloid analyses. Firstly, different fitting methods, to calculate the R_g from light scattering response, are evaluated for spherical latex beads and natural particles. The FlFFF–MALLS is then used to optimize FlFFF cross flow for best separation and minimal sample losses. Secondly, it is intended to elucidate the application of the FIFFF–MALLS coupling to assess and minimize fractionation and size determination artifacts. Finally, it is intended to apply the methodology in characterizing colloidal soil extracts (particle size and shape) and to explain the role of carbonates on formation of colloidal dispersion and sedimentation processes.

2. Methods and materials

The FlFFF system used is a F1000 model Universal Fractionator (Fractionation, Salt Lake City, USA, now Postnova Analytics Europe, Landsberg, Germany). The channel dimensions are 29 cm in length, 2.5 cm in width and 254 μm in thickness. A 10 kD regenerated cellulose membrane (Postnova Analytics Europe, Landsberg, Germany) was used as the accumulation wall. 'Milli-Q' water (Millipore, Bedford, UK) with 0.025% sodium dodecylsulfonate, and 0.02% NaN_3 in composition, was used as a carrier solution. The cross flow was maintained with a Pharmacia P500 double piston pump and the carrier solution was delivered by a Hewlett-Packard HP1100 isocratic HPLC pump. The FlFFF separation conditions were: 1 and 1.5 ml min^{-1} channel flow and 0.3, 0.5 and 0.75 ml min^{-1} cross flow. Concentration measurements were performed with an HP1100 Hewlett Packed Fluorescence Detector (FLD). The detector was operated at 320 nm excitation and emission wavelengths and used as concentration detector in a scattering mode (nephelometric turbidity detection) [25].

The DAWN EOS (Wyatt Technology Corp., Santa Barbara, CA, USA) was directly coupled to FlFFF after FLD detection. The net scattered light intensity (Rayleigh ratio, R) was measured simultaneously at 15 different scattering angles θ from 15 to 160°. Detectors 1 and 2 (<15°) were not usable with aqueous carrier in flow cell and detector 12 (100°) was occupied by

a light fiber for dynamic light scattering measurements. FlFFF was coupled to different detectors (MALLS and FLD) as shown in Fig. 1.

The ASTRA 4.73 software was used to collect signals from the FLD and MALLS detectors from which the R_g and its distribution can be calculated. Nanospherical polystyrene polymer standard particles (Duke Scientific, Palo Alto, CA) of sizes 50 ± 2 nm, 73 ± 2.6 nm, 102 ± 3 nm, 150 ± 4 nm, 220 ± 6 nm, 343 ± 9 nm, 494 ± 4 nm hydrodynamic diameters were used for the FlFFF calibration. The standards were supplied as dispersion at a concentration of 10 g/l. Stabilized colloidal extracts, from a natural aquifer containing inorganic colloids (<500 nm in diameter at a concentration of 122 mg l^{-1}), were used as natural samples to investigate the effect of cross flow on particle fractionation by FlFFF.

Undisturbed soil cores were drilled close to the *Ihlenberg* landfill, *Mecklenburg-Western Pomerania*, Northern Germany. Soil colloids were extracted from a silty till type soil obtained at depths of 15 m. The extraction procedure is summarized in Fig. 2. Two samples, with different chemical treatments, were

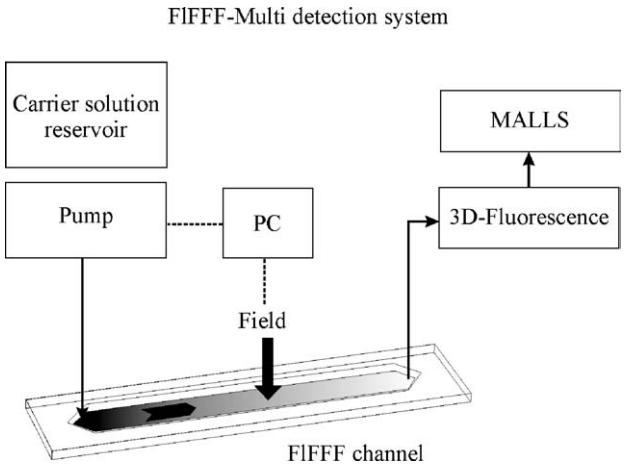

Fig. 1. Schematic diagram for the FlFFF-multi detection system (FFF–UV–DAD–LD–MALLS).

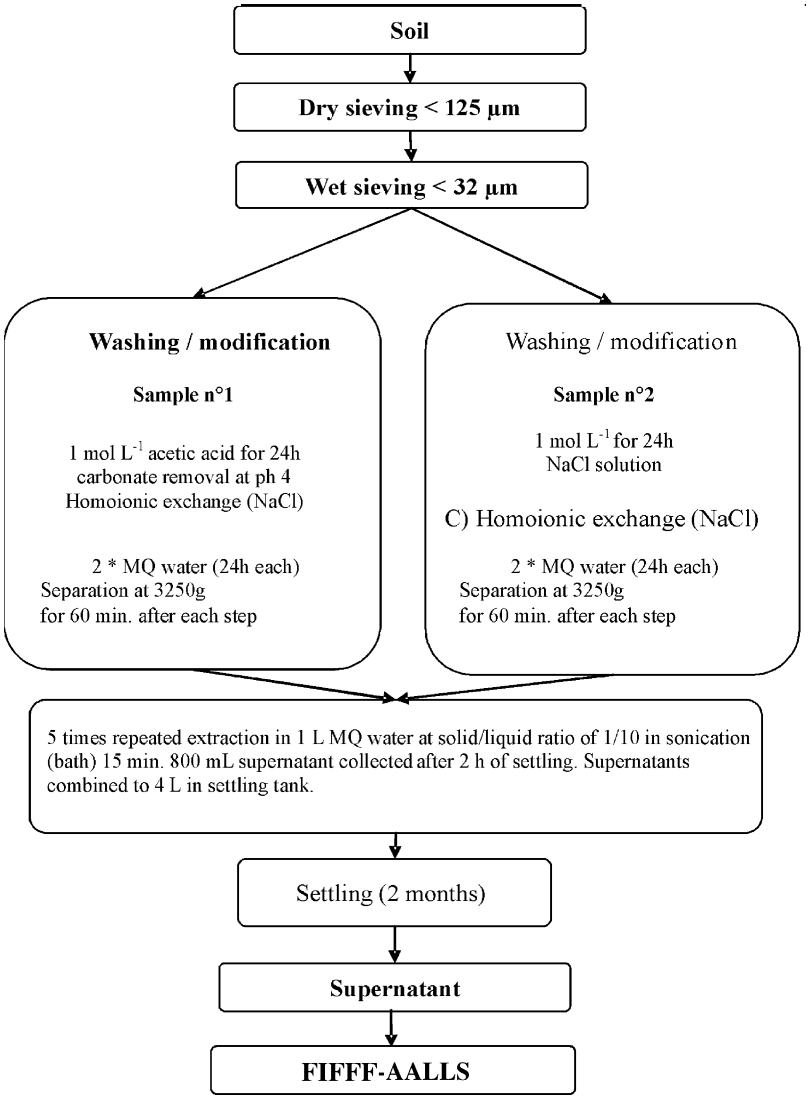

Fig. 2. A schematic procedure for soil extraction.

Table 1
Elemental composition (in mg l^{-1}) for different layers, for each sample, in each sedimentation tank

Sample	Layer number	Al	Si	Fe	Mn	Ca	Mg	Na	K
Sample 1	1	41.6	110	45.3	0.24	6.71	8.71	42.7	11.5
	2	69.5	174	73.6	0.4	9.5	14	42.6	20.1
	3	99	249	105	0.63	13.3	21	44.3	33.1
Sample 2	1	24.8	64.5	27.5	0.22	7.56	4.95	30	7.67
	2	46.7	117	51.6	0.44	11.1	9.41	31.2	14.7
	3	74.5	188	81.2	0.79	17.8	16.8	34.2	27.2

then prepared (sample nos. 1 and 2). Sample 1 was washed first with a (1.0 M) acetic acid/acetate buffer at pH 4 for 24 h, subsequently adjusting pH to 4 by adding hydrochloric acid (6.0 M) to dissolve the carbonate from the sample. The sample was then washed with NaCl (1.0 M) for 24 h, for homoionic exchange. Sample 2 was directly washed with NaCl (1.0 M) for 24 h for homoionic exchange without prior treatment with acetic acid. Both samples were then centrifuged at 3250 G for 60 min. The resuspended samples were left in 4 l polycarbonate bottles for 2 months to settle. Three optically different layers were identified in each sedimentation bottle after 2 months. An aliquot (10 ml) was taken from the middle of each layer by a syringe, equipped with a 25 cm long needle. Layer depths (from top of the bottle) were as follows: for sample no. 1: layer 1 at 9.5 cm, layer 2 at 13.5 and layer 3 at 20 cm; and for sample no. 2: layer 1 at 10 cm, layer 2 at 15 cm, and layer 3 at 20 cm. Sample elemental analysis was conducted on a Perkin-Elmer ELAN 6000 ICP-MS analyzer. Dionex ion-chromatography was conducted on the 0.45 μm filtration for major anions. Results are presented in Table 1. Chemical analysis shows that the composition, of the three layers in the two samples, is the same with Al/Si ratio between 0.38 and 0.40, Fe/Si ratio between 0.41 and 0.43 and negligible Mn relative to Fe, Al and Si. Therefore, other than calcium carbonate concentration in the source material, the sample compositions were not significantly affected by the treatment procedure.

3. Results and discussion

3.1. FlFFF calibration

Calibration experiments were conducted to correlate the hydrodynamical radius to the elution time of the FlFFF. Calibration was performed under several FlFFF operating conditions (cross flow = 0.3, 0.5 and 0.75 ml min^{-1}) using polymer standards. The standards were injected individually to the FlFFF channel and the corresponding retention volume V_{ret} was determined by subtracting the channel void volume from the peak elution volume of particle-size standard. Then, the relationship between particle hydrodynamic radius and FlFFF *elution volume* can be fitted by a linear function.

3.2. Fitting methods

In the limit of Rayleigh–Gans–Debye [11,26] the particle R_g may be determined from the slope of the net light scattering intensities as a function of scattering angle ($R(\theta)$ versus $\sin^2(\theta/2)$) at angle 0° [11,26–28]. Rigors of calculation procedures and relevant equations are described elsewhere [11,26–28]. The most critical point in R_g determination is the correct extrapolation of net light scattering intensities as a function of scattering angle ($R(\theta)$ versus $\sin^2(\theta)/2$) to angle 0°. Several fitting methods can be used to extrapolate the determined $R(\theta)$ to zero angle; among which are the Debye first, third and fifth order method and the Zimm method. The Zimm fitting function is based on extrapolation of the inverse of $R(\theta)$ to angle 0°, while Debye fitting method offers the possibility to use different polynomial fits (first, third and fifth degree). Details of these methods are described elsewhere [23,26].

3.2.1. Spherical particles

A mixture of seven nanospherical polymer standards, with different sizes in the range D_h = 50–494 nm, was used to investigate the light scattering variations with particle size and the different fitting methods to retrieve R_g from MALLS for standard spherical particles. Different particle concentrations were used, namely: 200 mg l^{-1} (50 nm), 100 mg l^{-1} (73 nm), 100 mg l^{-1} (102 nm), 80 mg l^{-1} (150 nm), 60 mg l^{-1} (220 nm), 40 mg l^{-1} (343 nm) and 20 mg l^{-1} (494 nm). The FlFFF fractogram for a channel flow of 1.5 ml min^{-1} and a cross flow of 0.75 ml min^{-1} is presented in Fig. 3. A discrete peak appears for each standard, although the two lowest standards (50 and 73 nm) elute without sufficient resolution. Fig. 3 also shows that small colloid

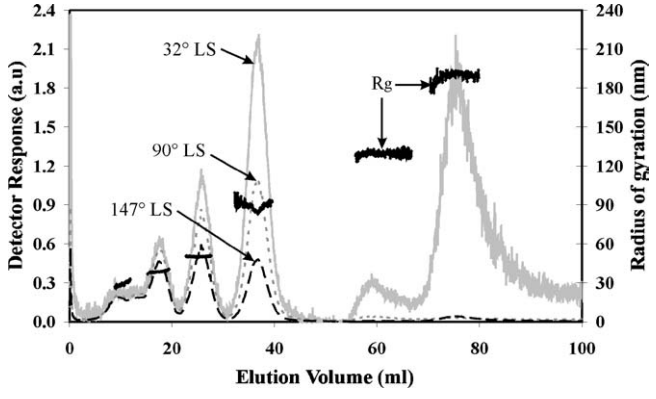

Fig. 3. Plots of light scattering (LS) responses (32, 90 and 147°) from a mixture of nanospherical standards, 50–494 nm, separated by FIFFF (channel flow = 1.5 ml min^{-1} and cross flow = 0.75 ml min^{-1}), together with plots of radius of gyration (R_g) vs. elution volume. The first two peaks are not very well separated and corresponds to 50 and 73 nm standards, the other five peaks are very well separated and correspond to 102, 150, 220, 343 and 494 nm standards.

Table 2
Comparison of the different Debye first, third and fifth fitting methods for calculating R_g of nanospherical standard particles with different sizes

Standard D_h (nm)	R_g (nm)			$D_h = 2R_g/0.775$ (nm)			E (%)		
	First	Third	Fifth	First	Third	Fifth	First	Third	Fifth
73	29.1	57.7	101	75.1	148.9	260.6	**2.9**	104.0	257.0
102	38.7	51.2	79.5	99.9	132.1	205.2	**2.1**	29.5	101.1
150	50.2	66.2	80.8	129.5	170.8	208.5	**13.6**	13.9	39.0
220	62	90.1	97.2	160.0	232.5	250.8	27.3	**5.7**	14.0
343	70.7	129.5	144.5	182.5	334.2	372.9	46.8	**2.6**	8.7
494	60.7	149.5	189.5	156.6	385.8	489.0	68.3	21.9	**1.0**

Values of hydrodynamic diameters, D_h, calculated hydrodynamic diameters, $D_h = 2R_h$, and relative errors, E, are shown. Note: The bold values indicate minimum error %.

particles, <150 nm, experience small differences in the scattered light intensity between the different scattering angles (32, 90 and 147°). Thus, small particles scatter light uniformly to the different angles. On the other hand, detector response variations increase as particle size increases implying a non-uniform scattering. From the results, the light scattering depends strongly on the particle size. These light scattering variations allow qualitative distinguishing between small and large particles during the FFF run. For quantitative size determination, several fitting methods were used to determine the R_g of the spherical standard particles (50, 73, 102, 150, 220, 343 and 494 nm) from the light scattering response, namely Debye first, third and fifth orders [11,26,28].

Table 2 shows the nominal hydrodynamic diameter for the standard, R_g, as determined from light scattering data by the Astra 4.73 program for each fitting method. The Table also shows the corresponding calculated diameter (D) using the relation ($R_g = 0.5\,(3/5)^{0.5}D$) for spherical particles, and the relative error between the standard and the calculated D. Results suggest that, for small spherical particles (50–150 nm) the Debye first order method gives the best fitting and the most appropriate calculation of the radius of gyration with a percentage error in the range 2.9–13.6%. For intermediate sizes (200–350 nm) Debye third order method gives the best fitting with a percentage of error in the range 2.6–5.7%. For larger particles the Debye fifth order method gives the best results (1% relative error). R_g values for different standards, calculated with the optimal method, are plotted against elution volume, as shown in Fig. 3. The results are consistent with earlier studies applying *Wyatt Dawn DSP* MALLS photometer [29]. Kammer et al. [28] comparatively evaluated the spherical particle model as included in ASTRAs particle mode, Zimm's, Debye's different orders and Berry's fitting methods. They found that for spherical particles, the spherical particle model and the Debye third order fitting method give the best results.

3.2.2. Natural samples

For natural colloidal samples, FlFFF fractogram (Fig. 4A) shows a continuous distribution. Due to natural colloid characteristics, it is not possible to compare the R_g obtained by the MALLS to any certified particle size standard. Thus, to determine the best fitting method, the Astra 4.73 allows applying different fitting methods as shown in Fig. 4B–E. The comparison between these fitting methods shows that, the Zimm first order gives the best data fitting. In addition, from earlier experience with natural colloidal samples, it was systematically noticed that, the Zimm first order is the best fitting method even for larger natural colloidal particles. This is in clear contradiction with the fact that the Zimm technique is only applicable to very small spherical particles below approximately 100 nm in diameter. This is probably related to the completely different light scattering behavior of natural particles, compared to spherical ones, which is due to the different shape of scattering pattern in function of the scattering angles ($P(\theta)$), for spheres and for natural particles (e.g. infinitely thin disks or fractal aggregates [25]). The latter are then better approximated by the first order Zimm fit [25].

The situation is demonstrated in Fig. 5. The angular intensity distribution, as retrieved from MALLS, is shown for spherical standards and natural colloidal particles of two identical R_g values. MALLS retrieves the R_g from the slope of the angular scattering function at zero angle. Therefore, the determined R_g quality depends on the extrapolation accuracy of $R(\theta)/Kc$ (Debye) or $Kc/R(\theta)$ (Zimm) to $\theta = 0°$, where K is a constant for a given instrument-particle system, and c is colloidal particle mass concentration. However, the determination of R_g is independent of c and the refractive index increment (dn/dc) incorporated in K. The scattering functions for small spherical particles may be fitted linearly (Zimm linear). However, the scattering function for large spherical particles cannot be fitted linearly, which imply the use of different order Debye fit as shown above. In natural particles $Kc/R(\theta)$ shows a linear behavior for small and large particles. Thus, the linear fit can be applied and it shows the best data fit (Fig. 4B–E). These results, together with those of Kammer et al. [28] demonstrate the applicability of MALLS for natural samples even for larger particle sizes. However, it must be stated that no absolute proof, for determined R_g value correctness, is available. This is due to the lack of well defined and characterized standards which resemble natural colloidal particle shape variations and polydispersity.

3.3. Effect of applied field strength on recovery and MALLS results

Cross flow is the major factor controlling the FlFFF fractionation and retention of particles. With natural colloidal particles, which are less stable than highly charged latex beads, the applied field must be balanced between effects of: poor retention, void-

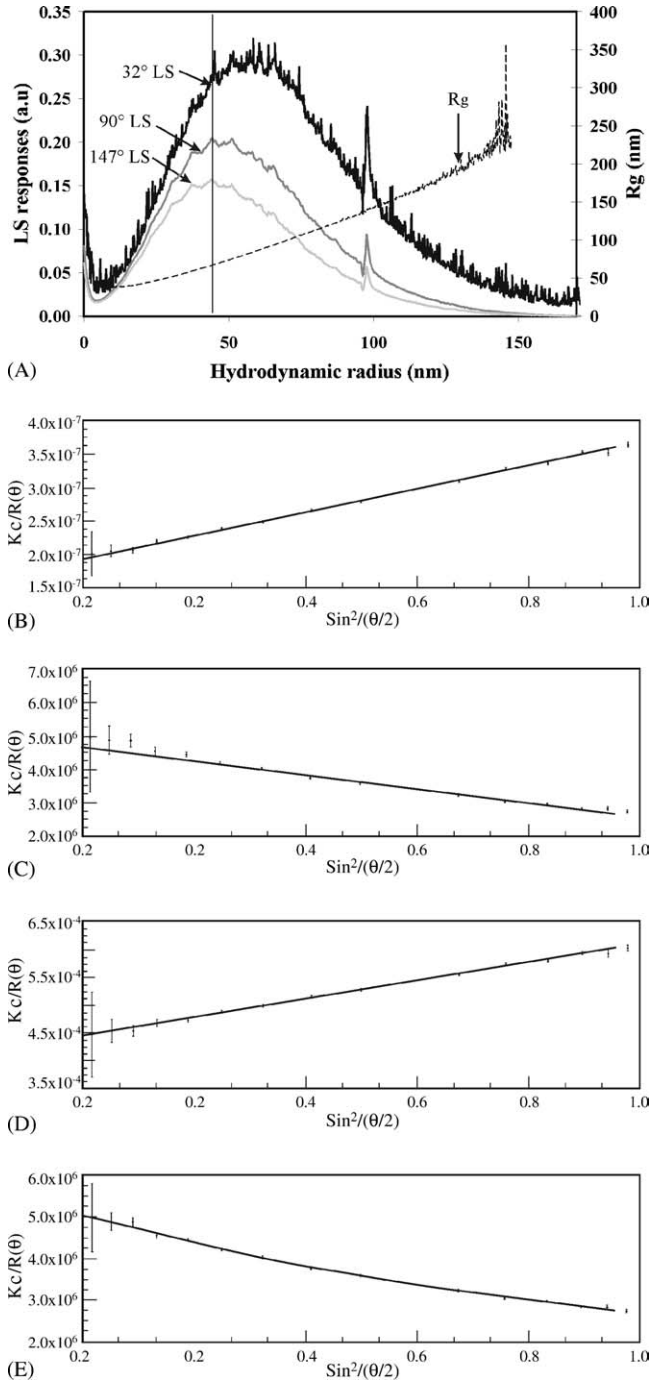

Fig. 4. (A) Plots of light scattering responses (32, 90 and 147°) from a natural colloidal sample (no. 1, layer 1) separated by FlFFF (channel flow = 1.0 ml min^{-1} and cross flow = 0.30 ml min^{-1}), together with plots of radius of gyration vs. hydrodynamic radius; (B) Zimm fitting; (C) Debye fitting; (D) Berry fitting and (E) Random coil fitting. The fittings in (B–E) are done for particle slice indicated by the vertical line in (A).

peak overlap (too low field force), and sample losses due to colloid-membrane interaction (too high field force). The cross flow effect on the fractionation of a stabilized colloid extract from an aquifer is shown in Fig. 6. In Fig. 6A, the *x*-axis represents retention volume, and in Fig. 6B, it represents the hydrodynamic diameter derived from the calibration obtained from nanospherical standard particles. The R_g was calculated from

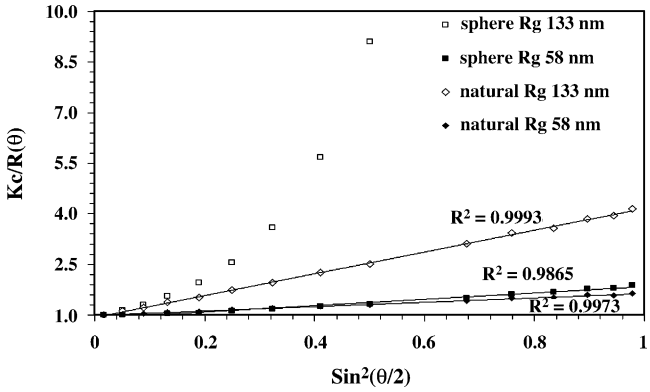

Fig. 5. Normalized light scattering responses for different nanospherical standards (R_h 25–247 nm) and different size fractions of a natural sample (see Fig. 4).

the MALLS using linear Zimm's fitting method as described above [28]. In all three experiments, the nearly linear behavior of R_g with retention volume is consistent with FlFFF theory. Fig. 6A and B shows that for a 0.3 ml min^{-1} cross flow rate (cf), the smallest detectable R_g near the void peak is elevated compared to other two experiments at higher cf rates. This indicates poor fractionation at low retention volume. Since the determined R_g is always a *z*-average, it can be assumed that larger particles present in the void peak may be carried over into the main sample peak region. The void peak may contain unretained particles

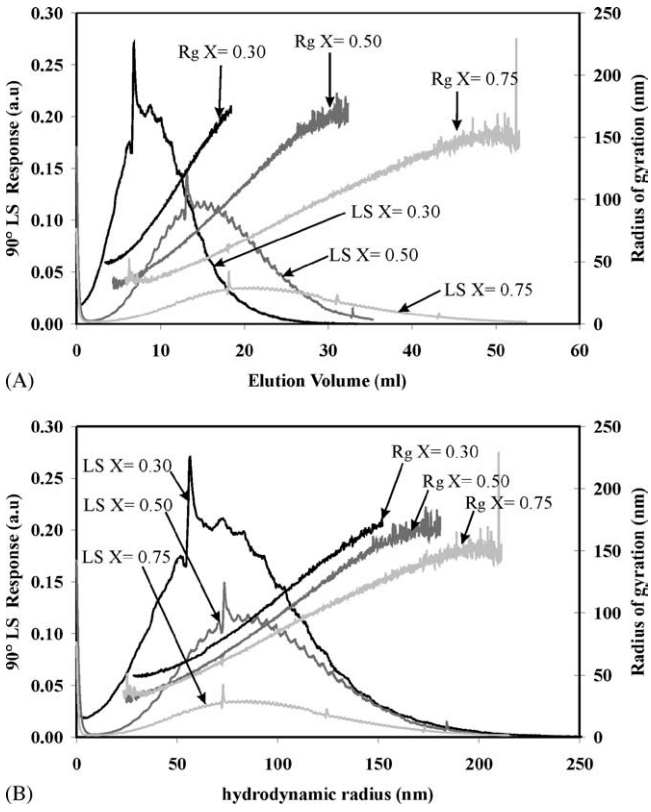

Fig. 6. Plots of 90° lazer light scattering response, together with radius of gyration vs. hydrodynamic radius, showing effect of cross flow on the fractionation of a stabilized extract of colloids, from an aquifer (120 mg l^{-1}). Fractionation conducted by FlFFF with cross flows of (0.3 ml min^{-1}, 0.5 ml min^{-1} and 0.75 ml min^{-1}) and a channel flow of 1 ml min^{-1}. Non-calibrated measurements (a) and calibrated measurements (b) are shown.

of possibly all sizes. For cf of 0.75 ml min^{-1}, the R_g fractionation near the void peak seems to be better. On the other hand, the largest R_g detected at the end of the signal peak is slightly smaller than values observed in other experiments. This indicates some selective losses of larger particles, most probably due to colloid–membrane interaction.

Fractionation with cf of 0.5 ml min^{-1} is as good as that with cf of 0.75 ml min^{-1}, which in turn is better than fractionation with cf 0.3 ml min^{-1}. Moreover, fractionation with cf of 0.5 ml min^{-1} shows a recovery that is comparable to that with cf of 0.3 ml min^{-1}, and better than that with cf of 0.75 ml min^{-1}. The recovery percentages are obtainable from division of the areas under peaks corresponding to 0.75 and 0.5 by that of 0.3 ml min^{-1}. Fig. 6A shows a recovery of 40% in case of 0.75 ml min^{-1} cross flow with respect to 0.3 ml min^{-1}, compared to 83% in case of 0.5 ml min^{-1} cross flow. Therefore, in MALLS analysis and recovery, cf of 0.5 ml min^{-1} seems to be an optimum cross flow under the described conditions for the respective sample. Thus, MALLS is a valuable technique to find optimum fractionation conditions.

Differences in the behavior of R_g over R_h (Fig. 6B) are due to several factors influencing the determination of both parameters. Variation in shape can presumably be excluded since it is not expected to have different particle shapes present in the same R_h slice simply by cross-flow variations. However, the remaining polydispersity in each sample fraction, analyzed by MALLS, is crucial since the determined R_g is a z-average of all sizes present in the fraction. The R_g is therefore shifted to larger values even by the presence of a small fraction of larger particles.

3.4. Sedimentation results

Three forces affect the sedimentation of colloids: gravity, buoyant force and the frictional force due to the viscous drag of the surrounding fluid. The gravity and the buoyant forces are directly proportional to colloids volume and density. The frictional force is related to particle size and shape. Particles with same equivalent spherical volume (D_h), but different shapes will be unequally affected. Thus, knowing particle shape is necessary to interpret sedimentation phenomenon [30]. Colloid size and shape of the three layers (top, mid and bottom) of samples nos. 1 and 2 were determined by FlFFF–MALLS (Figs. 7–9). The FlFFF conditions were chosen to be 1.0 ml min^{-1} channel flow and 0.3 ml min^{-1} cf. Fig. 7A shows three Gaussian-like size distribution peaks for sample no. 1. Fig. 7B displays the fractograms for sample no. 2 and shows three asymmetrical size distribution peaks shifted to larger particle size especially for the bottom layer. The size distribution (minimum, maximum, mean and standard deviation) based on light scattering response are summarized in Table 3. The R_g versus R_h plots, from FFF–MALLS, are shown in Fig. 7C and D. The R_g increases with increasing the R_h (elution volume). This confirms the FIFFF fractionation under constant field in Brownian mode. In sample no. 1, the increase of the slope at larger sizes indicates a change in particle composition or morphology.

The FlFFF–MALLS results (Fig. 7 and Table 3) show that in each sample, particle size varies for different layers, in the order: layer 3 > layer 2 > layer 1. Furthermore, these results show that sample no. 2 contains larger particles than those contained in

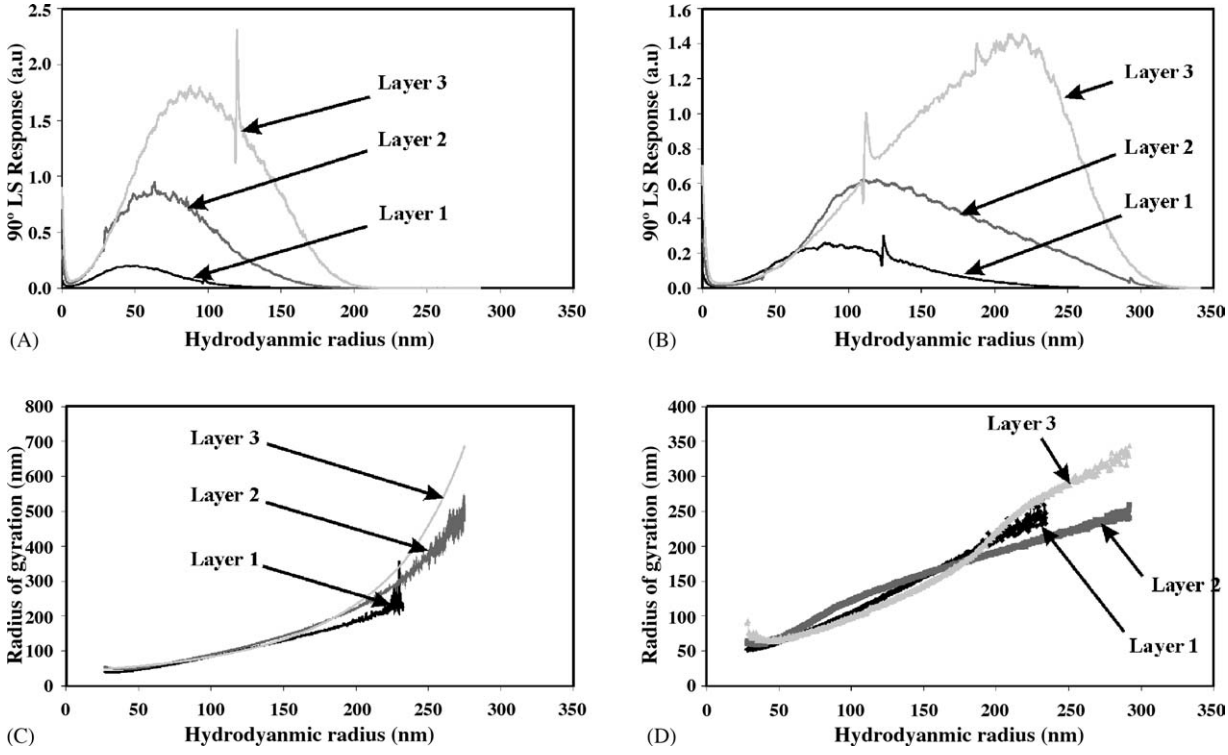

Fig. 7. Plots of 90° laser light scattering vs. radius of gyration, for each layer in sample no. 1 (A) and sample no. 2 (B), fractionated by FlFFF (channel flow = 1.0 and cross flow = 0.3 ml min^{-1}); together with plots of radius of gyration vs. hydrodynamic radius, for each layer in sample no. 1 (C) and sample no. 2 (D), calculated from light scattering.

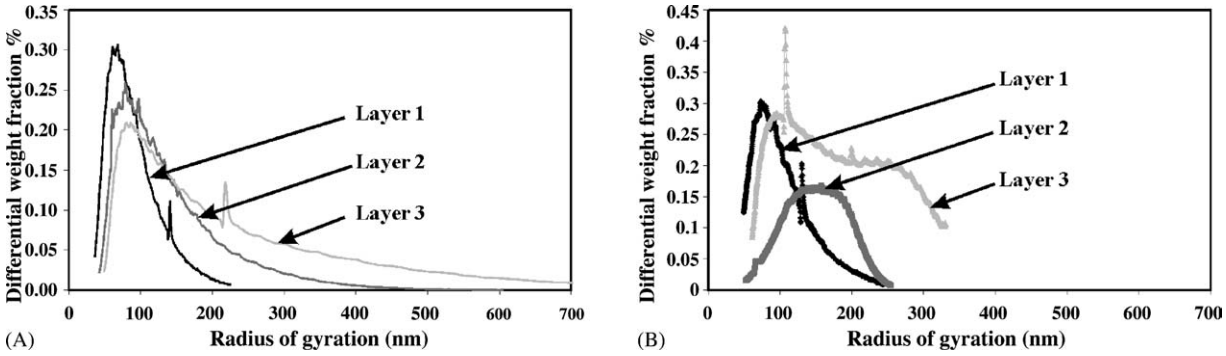

Fig. 8. Plots of percent differential weight distribution vs. radius of gyration for each layer in sample no. 1 (A) and sample no. 2 (B).

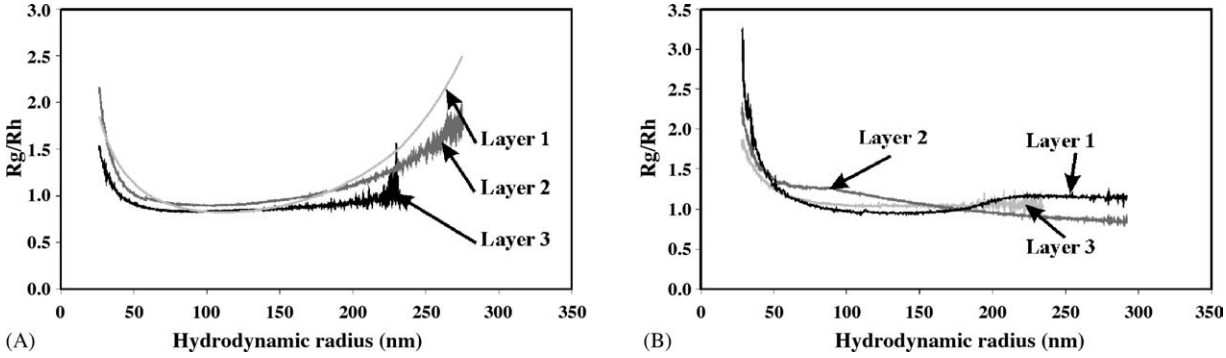

Fig. 9. Plots of shape factor (R_g/R_h) vs. hydrodynamic radius, for each layer, in sample no. 1 (A) and sample no. 2 (B).

sample no. 1. The large particles in sample no. 2 could be generated by the aggregation of colloidal particles as this sample was prepared without dissolving $CaCO_3$. Each layer in sample no. 2 contains larger particles (higher maximum and mean value of particle size) with higher polydispersity (higher standard deviation) than its counterpart in sample no. 1.

To generate size distributions from the determined R_g, a concentration detector such as UV–vis or FLD, is needed In this study, FLD was used in 90° light scattering mode [25] as a concentration detector to construct the differential weight distribution of the radius of gyration (Fig. 8A and B). The MALLS was used to calculate the R_g based on linear fitting of $Kc/R(\theta)$, and FLD was used as a proxy for particle mass concentration, assuming that the total area under the FLD response represents 100% of the sample.

Size distribution, minimum, maximum, mean and standard deviation, for each layer in both samples nos. 1 and 2, were obtained by calculating the R_g independently of the FlFFF, and are summarized in Table 4. In each sample, the particle size varies between different layers in the order: layer 3 > layer 2 > layer 1. This simply reflects the settling of particles in the sedimentation tanks. Sample no. 2 contains larger particles than those contained in sample no. 1. Additionally, each layer in sample no. 2 contains larger particles than those contained in the corresponding layer in sample no. 1. Thus, MALLS technique is convenient for colloids size determination, and its results are consistent with those obtained by FlFFF calibration with nanospherical standards of known size. The results are also consistent with colloidal particle fractionation order by FlFFF, viz. small particles elute first.

Fig. 8A and B shows that sample no. 1 contains a larger portion of fine colloidal particles (R_g < 150 nm) than sample no. 2 does. The percentage of fractions (fine <150, intermediate 150–200 and coarse colloidal particles >200 nm), calculated by integrating the areas under the curves for all particles in each size range, are summarized in Tables 5 and 6. For each sample, the

Table 3
Comparison between hydrodynamic radius distributions, within each layer, in each sample, showing minimum, maximum and mean values together with standard deviation

Layer number	Sample no. 1				Sample no. 2			
	Minimum	Maximum Mean	Mean	Standard deviation	Minimum	Maximum	Mean	Standard deviation
1	10	150	57	27	20	250	104	46
2	10	175	107	22	20	300	160	52
3	10	225	128	33	20	350	182	58

Data were calculated by means of descriptive statistical analysis of Fig. 7.

Table 4
Comparison between the radius of gyration distributions, within each layer, in each sample showing minimum, maximum and mean values together with standard deviation

Layer number	Sample no. l				Sample no. 2			
	Minimum	Maximum Mean	Mean	Standard deviation	Minimum	Maximum	Mean	Standard deviation
1	30	200	83	34	30	175	100	40
2	40	600	113	61	50	250	146	64
3	50	800	136	100	60	350	162	80

Data were calculated by mean of descriptive statistical analysis of Fig. 8.

Table 5
Percentage distributions of fine (<150 nm), intermediate (150–200), and coarse (>200 nm) colloidal particles sizes in each layer of sample no. 1

Layer number	Size range (nm)		
	<150	150–200	>200
1	95	4.20	0.80
2	81	10.50	8.50
3	73	10.59	16.41

Data were calculated by integrating the areas under the curves of Fig. 8A.

percentage, of the smaller particles, varies for different layers in the order: layer 1 > layer 2 > layer 3. This is due to the settling of particles in the sedimentation tanks, vide supra. Fig. 8A and B also shows higher portion of coarse particles (>200 nm) in sample no. 2 than in sample no. 1. This is assumable due to the higher $CaCO_3$ concentrations in sample no. 2, as manifested by the higher calcium concentrations therein (Table 1). As such, the carbonate works as cement causing adhesion between small particles and creating larger aggregates (>200 nm). Comparison, between the FlFFF calibration results (R_h) and light scattering MALLS (R_g) results, shows that for the sample no. 1 the hydrodynamic radius is less that the radius of gyration, while for sample no. 2 the hydrodynamic radius is larger than the radius of gyration. This variation is possibly due to variations in colloidal particles shapes in each sample. FlFFF–MALLS permits a particle shape assessment through calculating the R_g/R_h ratio, which describes particles shape variations from a solid sphere.

To better understand the sedimentation behavior of both samples, nos. 1 and 2, shape factor (R_g/R_h) was calculated and plotted versus hydrodynamic radius for all fractionated colloids (Fig. 9A and B). At the beginning of separation, R_g/R_h is determined unexpectedly high. This behavior can be explained by the influence of unretained large particles in the void peak which stretches into the main peak region. This causes an overestimation of the radius of gyration for the small fractions due to the

Table 6
Percentage distributions of fine (<150 nm), intermediate (150–200), and coarse (>200 nm) colloidal particles sizes in each layer of sample no. 2

Layer number	Size range (nm)		
	<150	150–200	>200
1	90	10.11	0
2	40.5	47.15	12.35
3	53	14.15	32.85

Data were calculated by integrating the areas under the curves in Fig. 8B.

z-average character of the determined R_g. The shape factor for the three layers of sample no. 1, has the same value of 0.85 for different particle sizes (in the range 50–150 nm hydrodynamic diameter). This value is close to the typical shape factor of a sphere (0.775). For larger hydrodynamic radius ranges, the shape factor increases to higher values 1.05, 2 and 2.7 for layers 1–3, respectively. The shape factor increases as soon as the particle deviates from a spherical shape toward, e.g. a platelet shape [25]. Therefore, in layers 2 and 3, particles deviate more from a spherical shape, as the particle size increases, than in layer 1. Sample no. 2 shows different behaviors. The shape factor here is approximately constant, with only little variation in the range 0.85 and 1.2. This indicates that the shape is closer to a sphere.

The variation in the shape factor, between sample nos. 1 and 2, may be attributed to an aggregation phenomenon that may occur due to higher carbonate ion concentrations in sample no. 2 than in sample no. 1. Platy particles may stick face-to-face, and thus, increase the overall particle thickness. As such, the resulting (aggregated) particles become less platy and tend to assume more spherical shape. The presence of some smaller fractions in the third layer, but not in the second layer, of the sample no. 2, is possibly due to desegregation of some small particles by the sonication process. This explains why washing with acetic acid, to dissolve the carbonate in sample no. 1 preparation, gives more homogeneous colloidal samples. Further investigation of the nature of aggregate formation, by cementation, needs to be conducted in the future. The study of the particle shape and nature of aggregation, using other techniques such as TEM, would be valuable.

4. Conclusions

This work demonstrates the applicability and benefits of FlFFF–MALLS in the analyses of natural colloidal particles. To calculate the R_g from light scattering response, different fitting methods are evaluated for spherical latex beads and natural particles. Results suggest that, for small (50–150 nm), intermediate (200–350 nm), and large (>350 nm) spherical particles, and for irregular shape natural colloidal particles; the Debye first, Debye third, and Debye fifth, and Zimm first are the best fitting methods, respectively.

MALLS measures the radius of gyration of fractionated particles independently of FlFFF operational parameters. MALLS has been used as a control technique of the FIFFF performance in case of complex natural samples. Artifacts in FIFFF fractionation, such as void peak overlap, particle interactions with the

membrane, steric inversion, and inside-channel particle aggregations, can be resolved with MALLS. Other methods such, as TEM and SEM, are potentially valuable control techniques, but FlFFF fractionation is still more advantageous in being easier, less time consuming and less costly.

FlFFF–MALLS is a valuable method to study the particle sedimentations. In addition to particle size fractionation and determination, it tells about deviation of particle shape from hard spheres. Such a parameter is necessary to understand the sedimentation process. Results show that, $CaCO_3$ (normally present in the environment of the colloids) may function as cement between the colloidal platy particles. This modifies particle shapes and changes their sedimentation behavior, as spherical particles settle faster than platy ones. Dissolution of $CaCO_3$ provides more homogeneous colloidal samples.

References

[1] J.F. McCarthy, Phys. Chem. Earth 23 (1998) 171.
[2] M.B. McGechan, Biosys. Eng. 83 (2002) 387.
[3] M.B. McGechan, D.R. Lewis, Biosys. Eng. 83 (2002) 255.
[4] A.L. Noell, J.L. Thompson, M.Y. Corapcioglu, I.R. Triay, J. Chromatogr. 31 (1998) 23.
[5] M.L. Wells, G.J. Smith, K.W. Bruland, Marine Chem. 71 (2000) 143.
[6] M.L. Wells, P.B. Kozelka, K.W. Bruland, Marine Chem. 62 (1998) 203.
[7] L. Denaix, R.M. Semlali, F. Douay, Environ. Pollut. 114 (2001) 29.
[8] Y. Ran, J.M. Fu, G.Y. Sheng, R. Beckett, B.T. Hart, Chemosphere 41 (2000) 33.
[9] M. Filella, J. Zhang, M.E. Newman, J. Buffle, Colloids Surf. A: Physicochem. Eng. Aspects 120 (1997) 27.
[10] R. Beckett, Z. Jue, C. Giddings, Environ. Sci. Technol. 21 (1987) 289.
[11] P.J. Wyatt, J. Colloid Interface Sci. 197 (1998) 9.
[12] C. Contado, G. Blo, F. Fagioli, F. Dondi, R. Beckett, Colloids Surf. A: Physicochem. Eng. Aspects 120 (1997) 47.
[13] M. Hassellöv, B. Lyvén, R. Beckett, Environ. Sci. Technol. 33 (1999) 4528.
[14] J.F. Ranville, D.J. Chittleborough, F. Shanks, R.J.S. Morrison, T. Harris, F. Doss, R. Beckett, Anal. Chim. Acta 381 (1999) 315.
[15] D.M. Murphy, J.R. Garbarino, H.E. Taylor, B.T. Hart, R. Beckett, J. Chromatogr. 642 (1993) 459.
[16] H.E. Taylor, J.R. Garbarino, D.M. Murphy, R. Beckett, Anal. Chem. 64 (1992) 2036.
[17] R. Chantiwas, R. Beckett, J. Jakmunee, I.D. McKelvie, K. Grudpan, Talanta 58 (2002) 1375.
[18] R. Beckett, D.M. Hotchin, B.T. Hart, J. Chromatogr. A 517 (1990) 435.
[19] R. Beckett, D. Murphy, S. Tadjiki, D.J. Chittleborough, J. Calvin Giddings, Colloids Surf. A: Physicochem. En. Aspects 120 (1997) 17.
[20] J.C. Giddings, in: M.E. Schimpf, K. Caldwell, J.C. Giddings (Eds.), Field Flow Fractionation Handbook, Wiley, New York, 2000, p. 3.
[21] L.J. Gimbert, K.N. Andrew, P.M. Haygarth, P.J. Worsfold, Trends Anal. Chem. 22 (2003) 615.
[22] R. Beckett, G. Nicholson, B.T. Hart, M. Hansen, J.C. Giddings, Water Res. 22 (1988) 1535.
[23] A. Zattoni, E. Loli Piccolomini, G. Torsi, P. Reschiglian, Anal. Chem. 75 (2003) 6469.
[24] US-EPA, Guidance Manual for Compliance with the Interim Enhanced Surface Water Treatment Rule: Turbidity Provisions, US-EPA Report, Office of Water, 1999, EPA 815-R-99-010.
[25] F.V.D. Kammer, M. Baborowski, K. Friese, J. Chromatogr. A 1100 (2005) 81–89.
[26] P.J. Wyatt, Anal. Chim. Acta 272 (1993) 1.
[27] P. Schurtenberger, M.E. Newman, in: J. Buffle, H.P. van Leeuwen (Eds.), Environmental Particles, vol. 2, Lewis Publications, Boca Raton, 1993.
[28] F. Kammer, M. Baborowski, K. Friese, Anal. Chim. Acta 552 (2005) 166.
[29] H. Thielking, D. Roessner, W.M. Kulicke, Anal. Chem. 67 (1995) 3229.
[30] B.R. Jennings, K. Parslow, Proc. R. Soc. Lond. A. 419 (1988) 137.